REVISION 1

New morphological, chemical, and structural data of woolly erionite-Na from Durkee, Oregon, USA

GEORGIA CAMETTI[1], ALESSANDRO PACELLA[1], FRANCESCO MURA[2], MARCO ROSSI[2,3], AND PAOLO BALLIRANO[1,*]

[1]Dipartimento di Scienze della Terra, Sapienza Università di Roma, Piazzale Aldo Moro 5, 00185 Roma, Italy.

[2]Centro di ricerca per le Nanotecnologie applicate all'Ingegneria della Sapienza (CNIS), Sapienza Università di Roma, Piazzale Aldo Moro 5, 00185 Roma, Italy.

[3]Dipartimento di Scienze di Base Applicate all'Ingegneria (SBAI), Sapienza Università di Roma, Piazzale Aldo Moro 5, 00185 Roma, Italy.

E-mail address: paolo.ballirano@uniroma1.it

ABSTRACT

A detailed morphological, crystal-chemical, and structural characterization of erionite from the type locality of Durkee, Oregon, has been carried out by combining field emission scanning electron microscopy (FESEM) and laboratory parallel-beam transmission X-ray powder diffraction (XRPD). According to the crystal-chemical formula $(Na_{5.38}K_{1.99}Mg_{0.24})[Al_{7.66}Si_{28.34}O_{72.09}] \cdot 29.83H_2O$, the sample has been classified as erionite-Na. The Rietveld refinement has indicated that the extraframework cations are located at three Ca1, Ca2, and Ca3 sites, the first one containing all available Mg. Moreover, it has been proved the absence of the additional K2 site found in both

dehydrated erionite and erionite-K. Notably, despite many works have reported the presence of a variable Fe and Ca content in erionite samples from Durkee, our results revealed the absence of both these elements. This is relevant information because it is well known from amphibole asbestos that Fe^{2+} has been claimed to be one of the causes of carcinogenesis by participating in Fenton chemistry and producing free radicals.

Keywords: Erionite-Na, Durkee Oregon, woolly morphology, crystal-chemistry, crystal structure, Rietveld method, Scanning Electron Microscopy, laboratory parallel-beam transmission X-ray powder diffraction.

Introduction

Erionite is a fibrous zeolite belonging to the so-called ABC-6 family (Gottardi and Galli 1985). It usually occurs in volcanic ash altered by weathering processes. From the structural point of view, it is hexagonal, space group $P6_3/mmc$. The erionite framework, topological code [ERI] (Meier and Olson 1992), consists of $(Si,Al)O_4$ tetrahedra linked together to form single-six rings (S6R) and double six-rings (D6R). S6R originate erionite cages by bridging adjacent columns at the level of the cancrinite (ε) cages. D6R connect columns of ε cages along the *z* direction. An average chemical formula $K_2(Na,Ca_{0.5})_8[Al_{10}Si_{26}O_{72}] \bullet 30H_2O$ has been proposed for erionite by Coombs et al. (1997). However, due to a significant chemical variability, three different species, erionite-K, erionite-Ca, and erionite-Na have been identified, depending on the most abundant extra-framework (EF) cation.

In the past few years fibrous erionite has been thoroughly investigated because of its linking with malignant mesothelioma (MM). In fact, *in vivo* studies unambiguously proved that erionite is several times more tumorigenic than chrysotile and crocidolite asbestos. As a consequence of this, the International Agency for Research on Cancer (IARC) listed erionite as a Group 1 Human-Carcinogen (IARC 1987, 2011). Erionite toxicity has been partly ascribed to the presence of ion-exchanged and/or surface deposited iron participating to Fenton chemistry and generating reactive oxygen species that induce DNA damage (Eborn and Aust 1995). In fact, despite erionite is a nominally Fe-free phase, Fe_2O_3 contents up to 3 wt% have been reported (Eberly 1964; Dogan et al. 2006). Besides, Dogan et al. (2006) reported that erionite from Rome (Oregon, USA) has a Fe_2O_3 content even higher than the Cappadocia erionite, the latter being responsible for the malignant mesothelioma epidemic. Ballirano et al. (2009) carried out a combined spectroscopic and crystal-chemical investigation of erionite-K from Rome hypothesizing that iron resides on the zeolite surface under the form of oxide-like nanoparticles with dimensions spanning from 1 to 9 nm. Notably, it was proposed that even upon inhalation of Fe-free fibers, they could imbibe Fe via ion exchange because protein injury can lead to metal ion release (Carr and Frei 1999). In any case,

whether Fe is carried on from erionite or is captured in the lungs, it was highlighted that the Fenton chemistry occurs on the surface of the fibers and that the coordination state of Fe^{2+} and Fe^{3+} is critical for inducing cytotoxicity and genotoxic damage (Fach et al. 2003; Ruda and Dutta 2005).

Several recent researches aimed at the investigation of fibers toxicity have been dedicated to the study of their surface reactivity, mainly by XPS analysis (Fantauzzi et al. 2010; 2012). The success of those investigations is strongly dependent on a fine crystal-chemical and structural characterization of the fibers. Coherently, a relevant effort has been devoted to improve the reliability of the chemical data extracted from micro-analytical investigations carried out through Transmission Electron Microscopy (TEM) (Dogan 2011), Scanning Electron Microscopy (SEM) (Dogan and Dogan, 2008), and Electron MicroProbe Analysis (EMPA) (Lowers et al. 2010) to properly constraint XPS experiments. This task is inherently very difficult for fibers and especially for zeolites because of, a part of the well-known problems related to the small dimensions, their instability under the electron beam that generally led to fairly reliable analytical results. As far as the structural characterization of fibers is concerned to, a significant number of papers fully exploiting the capabilities of laboratory parallel-beam transmission X-ray powder diffraction have been recently published (Ballirano et al. 2008; Pacella et al. 2008; Andreozzi et al. 2009; Ballirano et al. 2009; Ballirano and Cametti 2012). Such instrumental set up coupled with the preparation of the sample as a capillary mount allows an almost complete removal of preferred orientation significantly improving the reliability of the structural data even at non-ambient conditions (Ballirano 2011a,b,c).

The present study is dedicated to the detailed crystal-chemical characterization of a sample of woolly erionite from the type locality near Durkee, Oregon (USA), by combining data from X-ray powder diffraction (XRPD) and SEM analysis. The reported results are expected to provide a sound background for incoming experiments aimed at understanding the relationships occurring among morphology, crystal chemical and structural features, and biological activity of erionite.

EXPERIMENTAL METHODS

Scanning Electron Microscopy (SEM)

The analyzed erionite sample was provided by the Smithsonian Institution, Washington (NMNH R4066-1). At Durkee, Oregon, USA, erionite occurs in thin seams in gray, rhyolitic welded ash-flow tuffs (Sheppard 1996). The hand specimen consists of ribbons and bundles aggregating to form a hank having a white color and pearly luster as reported by Eakle (1898). SEM images were collected at the Centro di ricerca per le Nanotecnologie applicate all'Ingegneria della Sapienza (CNIS) using a field emission SEM (FESEM) Zeiss Auriga 405 with an accelerating voltage in the range 1.3-6 kV at a working distance in the range 2.8-3.5 mm. A preliminary set of chemical analyses was collected on bundles of erionite fibers. Moreover, two samples were prepared for a micro-chemical characterization by dispersing a small aliquot of fibers in distilled water in a beaker and subsequently pipetting and depositing a few droplets of the dispersion onto two aluminum stubs with double adhesive carbon tape. One of the stubs was coated with carbon, the other with gold, to check the possible occurrence of analytical differences arising from the coating. Analyses were collected for each stub positively verifying that the analytical results are independent from the coating type. The micro-chemical characterization was performed at the Dipartimento di Scienze della Terra, Sapienza Università di Roma using a FEI Quanta 400 SEM equipped with an EDX Genesis EDS system. Operating conditions were: 15 kV accelerating voltage, 11 mm working distance, 0° tilt angle. Chemical data were collected at thirty analytical points. The final crystal chemical formula was calculated, after renormalization of the chemical analyses hypothesizing a water content of 18.5 wt% (corresponding to *ca*. 30 atoms per formula unit, *apfu*), on the basis of 36 (Si+Al+Fe^{3+}) *apfu*.

In order to evaluate the quality of SEM-EDX microchemical data we performed a preliminary, thorough comparison with EMPA, using a fairly large prismatic erionite-Ca crystal as a standard. The sample, from Faedo, Colli Euganei, Italy, is a crystal of the same batch investigated by EMPA by Passaglia and Tagliavini (1995). Compositions were determined using a Cameca SX50 electron

112 microprobe with the following conditions: 10 s counting time (peak), 5 s counting time
113 (background), beam diameter 20 μm, excitation voltage 15 kV, specimen current 20 nA,
114 wavelength-dispersive spectrometry (WDS). The following standards were used: wollastonite (Si
115 and Ca), rutile (Ti), corundum (Al), magnetite (Fe), metallic Mn (Mn), barite (Ba), celestine (Sr),
116 periclase (Mg), orthoclase (K), and jadeite (Na). The raw data were corrected on-line for drift, dead
117 time, and background; matrix correction has been performed with a standard ZAF program. Results
118 of the chemical analyses are compared in Table 1. As can be seen, no relevant difference were
119 observed among the three data sets, the SEM-EDX being characterized by a very marginal increase
120 of the data dispersion indicating the full reliability of the technique. At any case, we unsuccessfully
121 attempted to prepare a sample of erionite from Durkee for EMPA analysis by embedding in epoxy
122 small hanks of fibers. Unfortunately, the polishing procedure unavoidably produced the separation
123 of the fibrils resulting in irregular, unpolished, surfaces. As a consequence, the resulting EMPA
124 cannot be considered as reliable.
125

126 **X-ray Powder diffraction (XRPD)**

127 Bundles of fibers were selected under a binocular microscope on the basis of the absence of any
128 recognizable impurity phase. They were subsequently disaggregated using a knife and carefully
129 hand-ground, under ethanol, in an agate mortar. The powder was loaded in a 0.7 mm diameter
130 borosilicate capillary that was aligned onto a standard goniometer head. XRPD data were collected,
131 up to a $(\sin\theta/\lambda)_{max}$ of 0.619 $Å^{-1}$, using a parallel-beam Bruker AXS D8 Advance Diffractometer,
132 operating in θ-θ geometry, equipped with Göbel mirrors on the incident beam, Soller slits on both
133 incident and (radial) diffracted beams, and a PSD VANTEC-1 detector. Experimental details of the
134 XRPD data collection are reported in Table 2. A careful scrutiny of the diffraction pattern confirmed
135 the absence of any detectable crystalline impurity, within the limits of the diffractometer sensitivity,
136 which is estimated to be of ca. 0.1 wt%. The structural refinement was carried out by the Rietveld
137 method using TOPAS v.4.2 (Bruker AXS 2009) running in launch mode. Peak shape was modeled

138 through FPA (Fundamental Parameters Approach), imposing the following full axial parameters:
139 divergence slit: 0.3°, source length 12 mm, sample length and receiving slit length 15.3(2) mm. The
140 starting structural model, taken from Alberti et al. (1997), consists, a part of the framework atoms,
141 of four EF cationic sites, K1, Ca1, Ca2, and Ca3; and six water molecules sites (OW7, OW8, OW9,
142 OW10, OW11, and OW12). Both the occupancy of all EF cationic and water molecules sites and
143 the displacement parameters of all sites were refined. However, because of the occurrence of
144 correlations, displacement parameters of the sites were constrained, according to the structural data
145 of Ballirano et al. (2009), as follow: $B_{T1} = B_{T2}$; $B_{O1} = B_{O2} = B_{O3} = B_{O4} = B_{O5} = B_{O6}$; $B_{Ca1} = B_{Ca2} =$
146 B_{Ca3}; $B_{Ow8} = B_{Ow9} = B_{Ow10} = B_{Ow11} = B_{Ow12} = 2*B_{Ow7}$. Absorption was modeled following the Sabine
147 model for cylindrical samples (Sabine et al. 1998) and the background was fitted by a Chebychev
148 polynomial of the first kind. The occurrence of preferred orientation was tested by means of
149 spherical harmonics (four refinable parameters up to the 6^{th} order). The choice of the number of
150 terms to be used has been performed following the procedure described by Ballirano (2003). As
151 expected for a capillary mount, only a marginal improvement of the fit was observed as a result of
152 the nearly absence of texture. A first refinement was carried out considering an isotropic shape of
153 the crystallites. The refinement smoothly converged to the following agreement indices: R_{wp} =
154 4.92%, R_p = 3.44%, R_B = 0.89% (Young 1993). However, a careful scrutiny of the Rietveld plots
155 (Figure 1a) indicated an imperfect fitting of the shape of a few peaks due to the strongly anisotropic
156 shape of the crystallites. Therefore, a second refinement was performed using the recently proposed
157 ellipsoid-model of Katerinopoulou et al. (2012) describing the diffraction-vector dependent
158 broadening of diffraction maxima. In the hexagonal symmetry, the shape ellipsoid parameters b_{ij} are
159 constrained as $b_{11} = b_{22} = 2b_{12}$; $b_{13} = b_{23} = 0$. The orientation of the ellipsoid is such that the
160 principal radii $r_a \perp c$ and $r_c \parallel c$. A significant improvement of the fit was obtained as compared to
161 the use of an isotropic shape of crystallites as indicated by the final agreement indices: R_{wp} = 3.36%,
162 R_p = 2.45%, R_B = 0.47%. Final Rietveld plots are shown in Figure 1b.
163

RESULTS AND DISCUSSION

Scanning electron microscopy (SEM)

From a morphological point of view, the sample consists of sub-parallel or bent bundles of fibers with woolly aspect. The diameter of the bundles ranges from 10 to 20 μm (Figure 2a). Each fiber is composed of very thin and curled fibrils as outlined in Figure 2b. The diameter of the fibers ranges from 0.3 to 2 μm, whereas that of a single fibril may be as small as 15 nm (Figure 2c). It is worth noting that as long fibers are tensile, elastic, and flexible, they are potentially extremely pathogenic upon inhalation because they cannot be phagocytized. The woolly aspect of the fibers is typical of the locality of Durkee, Baker County, as firstly reported by Eakle (1898). In addition, Gude and Sheppard (1981) described a woolly erionite sample from the Reese River deposit, Nevada, identical in appearance to that from Durkee. Notably, the morphology of both of these erionite is peculiar as it differs from that of erionite samples from other localities, which have been described as prismatic or acicular in habit.

The EDX spectra acquired on the bundles of fibers revealed, coherently with reference data, the occurrence of Ca, Mg, Na and, K as EF cations. In addition, a small amount of Fe content was detected (Figure 3). Moreover, preliminary semi-quantitative analyses pointed out that both CaO and Fe_2O_3 content widely differs depending on the analytical point, indicating a significant inhomogeneity of the sample. In particular, Fe_2O_3 and CaO content ranged from zero up to 4 wt%, and from zero up to 6 wt%, respectively. It must be noted that, as highlighted by FESEM images (Figure 2), it was very hard to discriminate and analyze a single fiber. For this reason a new set of analyses was carried out on isolated bundles obtained by dispersion in distilled water. In this case, the collected spectra clearly indicated the absence of both CaO and Fe_2O_3 (Figure 4). On this basis, the presence of these elements in the erionite fibers was ruled out and attributed to impurity phases. As confirmation of this, FESEM images revealed the presence of small particles of variable size (from 1 to 10 μm) and irregular shape resting at the fiber surface (Figure 5). Their chemical composition was qualitatively evaluated and the corresponding spectra showed that both Ca and Fe

190 are associated to these particles (Figure 6).

191 The reliability of the chemical analyses of the fibers was evaluated using both the balance error
192 formula E% (Passaglia 1970) and the Mg-content test (Dogan and Dogan 2008). Using the above-
193 mentioned experimental cautions, approximately 70% of the analyses passed both tests. The
194 average chemical composition is reported in Table 3. The MgO content did not exceed 0.54 wt%,
195 whereas Na resulted the most abundant EF cation with a Na_2O content ranging from 4.78 to 6.44
196 wt%. The final average crystal-chemical formula, calculated from 16 analytical point passing both
197 the E% and the Mg-content tests, of $(Na_{5.38}K_{1.99}Mg_{0.24})[Al_{7.66}Si_{28.34}O_{72.09}] \bullet 29.83H_2O$ allows a
198 sample classification as erionite-Na. The calculated R = Si/(Al+Si) ratio of 0.787 is identical to that
199 found by Passaglia et al. (1998) for the erionite sample no. 25 from Durkee. The abundance of Na
200 and the absence of Ca result in a very high M/(M+D) ratio of 0.97 (M = Na+K; D = Ca+Mg+Mn).
201 A similar value of M/(M+D) = 0.95, was previously found in only one of the large set of 25 erionite
202 samples analyzed by Passaglia et al. (1998) (sample no. 8 from Phillip Island, Australia). In fact, its
203 chemical composition, in term of EF cations, is very close to that of the erionite investigated in this
204 work the exception being a higher K_2O content. Besides, sample no. 25 from Durkee has a chemical
205 composition significantly different with respect to that of the present sample, and as a result, it can
206 be classified as erionite-Ca. Moreover, chemical data obtained in the present work significantly
207 differ with respect to those previously obtained on woolly erionite samples by various authors
208 (Eakle 1898; Staples and Gard 1959; Gude and Sheppard 1981). In particular, in the case of
209 erionite-Na from Durkee the $Si/(Al+Fe^{3+})$ ratio is significantly larger (reference samples do not
210 exceed 3.50 instead of 3.69 of the present sample) as well as the M/(M+D) ratio (less than 0.80 in
211 reference samples: Sheppard and Gude 1969).
212

213 **Structural refinement**

214 **Micro-structural parameters and framework**

215 Cell parameters *a* = 13.2356(5) Å and *c* = 15.0652(6) Å and cell volume V = 2285.6(2) $Å^3$ are

similar to those reported in Ballirano et al. (2009) for erionite-K from Rome, Oregon, as expected from the similar R value. A comparison with reference data of cell parameters of erionite samples from Durkee is reported in Table 4. A good agreement is observed with the data of Passaglia et al. (1998) for a sample characterized by an identical R value but a different EF cationic content. The cell parameters of Sheppard and Gude (1969) are systematically larger than those of both the present work and Passaglia et al. (1998). However, the *c/a* ratios are identical within 1σ.

From the refined anisotropic crystal shape parameters b_{11} and b_{33}, the principal ellipsoid radii r_a = 15.5(2) nm and r_c = 79(5) nm were computed using the relations $r_a = 1/(a \cos 30° \, b_{11}^{0.5})$ and $r_c = 1/(c \, b_{33}^{0.5})$, leading to a r_c/r_a ratio of 5.1(9). Moreover a ε_0 micro-strain (lattice strain) of 0.200(7) was obtained (Ballirano and Sadun 2009). For comparison purposes, the refinement with unique average crystallite size gave spherical crystallites with radius r = 30(1) nm and a ε_0 micro-strain of 0.207(12).

The r_a value is comparable with the diameter of a single fibril observed by FESEM. On the contrary, the coherency along the fiber axis is significantly shorter than the full length of the fibril. This is clearly an effect of the bending of the fibrils that reduces the coherency along the *c*-axis.

Fractional coordinates, isotropic displacement parameters, and site scattering (*s.s.*) are reported in Table 5, relevant bond distances and angles in Table 6, and bond valence analysis in Table 7.

The mean bond distances <T1-O> = 1.631 Å and <T2-O> = 1.646 Å clearly indicate a disordered Si/Al distribution (<T1-O> - <T2-O> = -0.015 Å) and the preferential partition of Al at the T2 site. The R ratio has been calculated by using both the Jones' determinative curves (Jones, 1968) and the regression equation of Passaglia et al. (1998). The population of the two T1 ($Al_{4.21}Si_{19.79}$) and T2 ($Al_{3.26}Si_{8.74}$) sites, determined using the Jones' determinative curve, provides an R value of 0.793. Besides, an R value of 0.783 has been obtained using the regression equation of Passaglia et al. (1998). Both values are reasonably close with that of 0.787 obtained from chemical data. On the contrary, the corresponding mean bond distances <T1-O> = 1.630 Å and <T2-O> = 1.705 Å obtained from the isotropic crystallite shape refinement seem to indicate a very strong preference of

Al for T2 ($Al_{7.80}Si_{4.20}$). However, the mean <T-O> bond distances result in an R value of 0.671, which is unsupported by both chemical and unit cell volume data. This result can be rationalized considering the deleterious effects of an imperfect peak-shape modeling on the accuracy of the structural parameters determination. Therefore, any effort has to be paid to adequately model the anisotropic broadening of diffraction maxima to extract reliable structural information from fibrous samples.

Extraframework cations

Chemical data indicate a total site scattering of 99.9 e^- for the EF cations. This value is in reasonable agreement with the *s.s.* of 98(4) e^- obtained from the Rietveld refinement (Table 5). Similarly, a total of 31.2(13) water molecules *pfu* has been obtained from the refinement, in good agreement with reference data (Coombs et al. 1997; Ballirano et al. 2009). Notably, the *s.s.* value of 100(5) e^- and 42(5) water molecules *pfu,* obtained in the isotropic crystallite shape refinement, confirm the fundamental role played by an accurate fitting of the peak shape for extracting reliable structural parameters.

The K atom lies at the K1 site located at the center of the cancrinite cage. The fully occupied site is 12-fold coordinated by six O2 atoms and six O3 atoms at 2.957(10) Å and 3.348(9) Å respectively (Table 6). For this site, bond valence analysis, performed using the parameters of Breese and O'Keeffe (1991), results in 0.86 valence units (*v.u.*) (Table 7). This site does not provide a favorable coordination for Na as indicated by bond valence analysis (0.36 *v.u.*). Therefore, reported values of less than 2 K *apfu* indicate a partly vacant K1 site or, more plausibly, an inaccurate chemical analysis. Attempts to detect the occurrence of electron density at the K2 site, located at the center of the boat-shaped 8-member rings (8MR) forming the walls of the erionite cage, failed. As reported in Ballirano et al. (2009), this site corresponds to that found by Schlenker et al. (1977) in dehydrated erionite and to the site labeled as Ca4 by Gualtieri et al. (1998) in two erionite samples. It has been shown that the K2 site provides a very favorable coordination for K

268 atoms at room temperature. However, in our case the available K is entirely located within the
269 cancrinite cages and, as a consequence of this, the K2 site is empty. The remaining EF cationic sites,
270 Ca1, Ca2 and Ca3, are located at (1/3, 2/3, *z*), along the three-fold axis. These sites were refined
271 using the Mg scattering factor for the Ca1 site and the Na scattering factor for the Ca2 and Ca3
272 sites, following the same approach adopted by Ballirano et al. (2009) for erionite-K from Rome.
273 Atomic fractional coordinates and displacement parameters are reported in Table 4. Values are in
274 good agreement with those reported for erionite-K from Rome in Ballirano et al. (2009), and those
275 reported for erionite-Ca from Tunguska (Russia) by Alberti et al. (1997). Differences in both *s.s.*
276 and population of the EF cationic sites are clearly related to the different chemical composition. The
277 Ca1 site has a very low *s.s.* of 5.4(14) e^- and the associated high standard deviation of bond and
278 contact distances render difficult a meaningful discussion about its coordination and site
279 assignment. However, it has been identified a fairly regular six-fold coordination (Ca1-OW8 x3 at
280 1.88(9) Å and Ca1-OW10 x3 at 2.68(12) Å) well fitting the occurrence of Mg (Table 6). This
281 assignment is confirmed by a bond-valence sum of 2.03 *v.u*. The value of 0.24 *apfu* obtained from
282 chemical analysis for Mg corresponds to a *s.s.* value of 2.9 e^-. It is worth noting that, this value is in
283 reasonable agreement with the results obtained from the structural refinement, under the hypothesis
284 that all Mg content is located at Ca1, as in the case of erionite-K (Ballirano et al. 2009). However,
285 the coordination of Mg is different in erionite-Na and –K as both Ca1 and Ca2 sites in erionite-K
286 are slightly displaced off-axis, and the OW9 water molecule site is significantly displaced in
287 erionite-Na as compared to both erionite-K and -Ca (Alberti et al., 1997). Therefore, Na is located
288 at both Ca2 and Ca3 sites. The Ca2 site has the largest *s.s.* value (35.5(10) e^-) among the three EF
289 cationic sites located within the erionite cage. It is characterized by a nine-fold coordination (Ca2-
290 OW8 x3 at 2.54(4) Å, Ca2-OW12 x3 at 2.68(3) Å, and Ca2-O5 x3 at 3.376(19) Å) leading to a
291 bond-valence sum of 0.72 *v.u*. The Ca3 site, not occurring in erionite-K, is at bonding distance with
292 OW7, OW10, and OW11 sites. However, according to the bond-valence analysis and taking into
293 account the short non occurring contact OW7-OW11 (1.73(6) Å), a nine-fold coordination may be

proposed, consisting of Ca3-OW10 x 3 at 2.47(3) Å, Ca3-OW11 x3 at 2.64(7), and Ca3-OW10 x3 at 3.10(4) Å, leading to a bond valence sum of 0.90 *v.u*.

Concerning the water molecule positions, the most relevant difference with respect to Rome and Tunguska erionite samples is related to the displacement of OW9 (from x ca. 0.44, $y = 2x$; z = ca. 0.92 to x ca. 0.50, $y = 2x$; z = ca. 0.95).

Water molecules site scattering of erionite-K and -Na are similar, a part for an inversion between neighboring OW8 and OW9 sites.

On the contrary, differences are very relevant with respect to erionite-Ca (Alberti et al. 1997). Besides, in the case of the present erionite-Na sample, OW9 is linked exclusively to framework oxygen atoms and other H_2O molecules differently from OW8, OW11, and OW12 of erionite-K (Ballirano et al. 2009).

Environmental and health relevance

Despite many works have reported the presence of a variable Fe and Ca content in erionite samples from Durkee, our results revealed the absence of both these elements. In particular, the absence of Fe, confirming the findings of Ballirano et al. (2009) for erionite-K from Rome, it is of relevant interest because it is well known from amphibole asbestos that Fe has been claimed to be one of the causes of carcinogenesis by participating in Fenton chemistry and producing free radicals (e.g., Kane et al. 1996; Fubini and Otero Aréan 1999; Kamp and Weitzman 1999; Robledo and Mossman 1999). Notably, it was proposed that, in addition Fe presence, erionite ion exchanging could play a primary role to induce toxicity (Eborn and Aust 1995). In fact, cations may be readily exchanged whenever a zeolite is in contact with human body fluids. It is worth noting that Ballirano and Cametti (2012) have shown that Mg in Ca1 is the most mobile cation during heating of erionite-K, despite its large ionic potential. Notably, results of *in vitro* experiments on amphibole asbestos revealed that the release of Mg^{2+} can have different effects on lipid packing, membrane permeability and can counteract Ca^{2+} uptake by blocking the calcium uniporter (Bergamini et al.

2007; Pacella et al. 2012). Further studies are in progress on the erionite sample here studied, concerning the exchange properties of erionite in contact with a physiological solution and the reactivity (detection of oxy-radicals and monitoring of lipid peroxidation). The combined approach consisting in the full characterization of the fibrous erionite coupled with the cation exchange properties and reactivity studies is very promising to shed new light on the role of the ion exchange in the interaction between fibers and organic environment.

Besides, the possible role of erionite as a carrier within the human body for nanoscale iron-bearing materials needs to be carefully investigated.

Acknowledgments

We thank M. Serracino and M. Albano for help and assistance during EMPA and SEM analyses. We are grateful to dott. Arnoldo Melli and prof. Elio Passaglia for providing the crystal or erionite-Ca from Faedo. We also aknowledge referees, Heather A. Lowers and an anonymous reviewer, and Richard Yuretich, the associate editor, for their helpful comments and critiques, which greatly improved the manuscript. The work has received financial support from Sapienza Università di Roma.

REFERENCES

Alberti, A., Martucci, A., Galli, E., and Vezzalini, G. (1997). A reexamination of the crystal structure of erionite. Zeolites, 19, 349-352.

Andreozzi, G.B., Ballirano, P., Gianfagna, A., Mazziotti-Tagliani, S., and Pacella, A. (2009) Structural and spectroscopic characterization of a suite of fibrous amphiboles with high environmental and health relevance from Biancavilla (Sicily, Italy). American Mineralogist, 94, 1333-1340.

Ballirano, P. (2003) Effects of the choice of different ionisation level for scattering curves and correction for small preferred orientation in Rietveld refinement: the $MgAl_2O_4$ test case. Journal of Applied of Crystallography, 36,1056-1061.

Ballirano, P. (2011a) Thermal behavior of natrite Na_2CO_3 in the 303-1013 K thermal range. Phase Transitions, 84, 357-374.

Ballirano, P. (2011b) Laboratory parallel beam transmission X-ray powder diffraction investigation of the thermal behavior of calcite: comparison with X-ray single-crystal and synchrotron powder diffraction data. Periodico di Mineralogia, 80, 123-134.

Ballirano, P. (2011c) Laboratory parallel beam transmission X-ray powder diffraction investigation of the thermal behavior of nitratine $NaNO_3$: spontaneous stress and structure evolution. Physics and Chemistry of Minerals, 38, 531-541.

Ballirano, P. and Cametti, G. (2012) Dehydration dynamics and thermal stability of erionite-K: Experimental evidence of the “internal ionic exchange” mechanism. Microporous and Mesoporous Materials, 163, 160-168.

Ballirano, P., Andreozzi, G.B., and Belardi, G. (2008) Crystal chemical and structural characterization of fibrous tremolite from Susa Valley, Italy, with comments on potential harmful effects on human health. American Mineralogist, 93, 1349-1355.

Ballirano, P., Andreozzi, G.B., Dogan, M., and Dogan, A.U. (2009) Crystal structure and iron

topochemistry of erionite-K from Rome, Oregon, U.S.A. American Mineralogist, 94, 1262-1270.

Ballirano, P. and Sadun, C. (2009) Thermal behavior of trehalose dihydrate (T_h) and β-anhydrous trehalose (T_β) by in-situ laboratory parallel-beam X-ray powder diffraction. Structural chemistry, 20, 815-823.

Bergamini C., Fato R., Biagini G., Pugnaloni A., Gaintomassi F., Foresti E., Lesci G. I., Roveri, N., Lenaz, G. (2007) Mitochondria changes induced by natural and synthetic asbestos fibers: studies on isolated mitochindria. Cell and Molecular Biology, 52(Supp), 691-700.

Breese, N.E. and O'Keeffe, M. (1991) Bond-valence parameters for solids. Acta Crystallographica, B47, 192-197.

Bruker AXS (2009) Topas V.4.2: General profile and structure analysis software for powder diffraction data. Bruker AXS, Karlsruhe, Germany.

Carr, A. and Frei, B. (1999) Does vitamin C act as a pro-oxidant under physiological conditions? The FASEB Journal, 13, 1007-1023.

Coombs, D.S., Alberti, A., Armbruster, T., Artioli, G., Colella, C., Galli, E., Grice, J.D., Liebau, F., Mandarino, J.A., Minato, H., Nickel, E.H., Passaglia, E., Peacor, D.R, Quartieri, S., Rinaldi, R., Ross, M., Sheppard, R.A., Tillmanns, E., and Vezzalini, G. (1997) Recommended nomenclature for zeolite minerals; report of the Subcommittee on Zeolites of the International Mineralogical Association, Commission on New Minerals and Mineral Names. Canadian Mineralogist, 35, 1571-1606.

CrystalMaker Software (2012) CrystalMaker 8.7. Bicester, Oxfordshire, England.

Dogan A.U., Baris Y.I., Dogan M., Emri S., Steele I., Elmishad A.G., and Carbone M. (2006) Genetic predisposition to fiber carcinogenesis causes a mesothelioma epidemic in Turkey. Cancer Research, 66, 5063-5068.

Dogan, A.U. and Dogan, M., (2008) Re-evaluation and re-classification of erionite series minerals. Environmental Geochemistry and Health, 30, 355-366.

Dogan, M. (2011) Quantitative characterization of the mesothelioma-inducing erionite series

minerals by Transmission Electron Microscopy and Energy Dispersive Spectroscopy. Scanning, 33, 1-6.

Eakle, A.S. (1898) Erionite, a new zeolite. American Journal of Science, 156, 66-68.

Eberly, P.E. (1964) Adsorption properties of naturally occurring erionite and its cationic-exchanged forms. American Mineralogist, 49, 30-40.

Eborn, S.K. and Aust, A.E. (1995) Effect of iron acquisition on induction of DNA singlestrand breaks by erionite, a carcinogenic mineral fiber. Archives of Biochemistry and Biophysics, 316, 507-514.

Fantauzzi, M., Pacella, A., Atzei, D., Gianfagna, A., Andreozzi, G.B., and Rossi, A. (2010) Combined use of X-ray Photoelectron and Mössbauer spectroscopic techniques in the analytical characterization of iron oxidation state in amphibole asbestos. Analytical and Bioanalytical Chemistry, v. 396, n. 8, p. 2889-2898.

Fantauzzi, M., Pacella, A., Fournier, J., Gianfagna, A., Andreozzi, G.B., and Rossi, A. (2012) Surface chemistry and surface reactivity of fibrous amphiboles that are not regulated as asbestos. Analytical and Bioanalytical Chemistry, 404, 821-833.

Fach, E., Kristovich, R., Long, J. F., Waldman, W. J., Dutta, P.K., and Williams, M.V. (2003) The effect of iron on the biological activities of erionite and mordenite. Environmental International, 29, 451-458.

Fubini, B. and Aréan Otero, C. (1999) Chemical aspects of the toxicity of inhaled mineral dusts. Chemical Society Reviews, 28, 373-381.

Gottardi, G. and Galli, E. (1985) Natural zeolites. Springer-Verlag, Heidelberg.

Gualtieri, A., Artioli, G., Passaglia, E., Bigi, S., Viani A., and Hanson, J.C. (1998) Crystal structure-crystal chemistry relationships in the zeolites erionite and offretite. American Mineralogist, 83, 590-606.

Gude, A.J. 3rd and Sheppard, R.A. (1981) Woolly erionite from the Reese River zeolite deposit, Lander County, Nevada, and its relationship to other erionites. Clays and Clay Minerals, 29, 5, 378-

384.

IARC (1987) IARC Monographs on the evaluation of the carcinogenic risk to humans. Silica and some silicates. Volume 42, 225-239.

IARC (2011) IARC Monographs on the evaluation of the carcinogenic risk to humans. Arsenic, metals, fibres and dusts. Volume 100 C, 311-316.

Jones, J.B. (1968) Al-O and Si-O tetrahedral distances in aluminosilicate framework structures. Acta Crystallographica, B24, 355-358.

Kamp, D.W. and Weitzman, S.A. (1999) The molecular basis of asbestos induced lung injury. Thorax, 54, 638-652.

Kane, A.B., Boffetta, P., Saracci, R., and Wilbourn, J.D. (1996) Mechanisms of fibre carcinogenesis, 157 p. IARC Scientific Publication 140, Lyon, France.

Katerinopoulou, A., Balic-Zunic, T., and Lundegaard, L.F. (2012) Application of the ellipsoid modeling of the average shape of nanosized crystallites in powder diffraction. Journal of Applied Crystallography, 45, 22-27.

Lowers, H.A., Adams, D.T., Meeker, G.P., and Nutt, C.J. (2010) Chemical and morphological comparison of erionite from Oregon, North Dakota, and Turkey. U.S. Geological Survey Open-File Report 2010-1286, 13 pp.

Meier, W.M. and Olson, D.H. (1992) Atlas of zeolite structure types. Zeolites, 12, 449-656.

Pacella A., Andreozzi, G.B., Ballirano, P., and Gianfagna, A. (2008) Crystal chemical and structural characterization of fibrous tremolite from Ala di Stura (Lanzo Valley, Italy). Periodico di Mineralogia, 77, 51-62.

Pacella, A., Andreozzi, G.B., Fournier, J., Stievano, L., Giantomassi, F., Lucarini, G., Rippo, M.R., and Pugnaloni, A. (2012) Iron topochemistry and surface reactivity of amphibole asbestos: relations with in vitro toxicity. Analytical and Bioanalytical Chemistry, 402, 871-881.

Passaglia, E. (1970) The crystal chemistry of chabazites. American Mineralogist, 55, 1278-1301.

Passaglia, E., Artioli, G., and Gualtieri, A. (1998) Crystal chemistry of the zeolites erionite and

441 offretite. American Mineralogist, 83, 577-589.

442 Robledo, R. and Mossman, B. (1999) Cellular and molecular mechanisms of asbestos-induced
443 fibrosis. Journal of Cellular Physiology, 180, 158-166.

444 Ruda, T.A. and Dutta, P.K. (2005). Fenton chemistry of Fe^{III} -exchanged zeolitic minerals treated
445 with antioxidants. Environmental Science and Technology, 39, 6147-6152.

446 Sabine, T.M., Hunter, B.A., Sabine, W.R., and Ball, C.J. (1998) Analytical expressions for the
447 transmission factor and peak shift in absorbing cylindrical specimens. Journal of Applied
448 Crystallography, 31, 47-51.

449 Schlenker, J.L., Pluth, J.J., and Smith, J.V. (1977) Dehydrated natural erionite with stacking faults
450 of the offretite type. Acta Crystallographica, B33, 3265-3268.

451 Sheppard, R.A. (1996) Occurrences of erionite in sedimentary rocks of the Western United States.
452 U.S. Geological Survey Open-File Report 96-018, 24 pp.

453 Sheppard, R.A. and Gude A.J. 3rd (1969) Chemical composition and physical properties of the
454 related zeolites offretite and erionite. American Mineralogist, 54, 875-886.

455 Staples, L.W. and Gard, J.A. (1959) The fibrous zeolite erionite: its occurrence, unit cell, and
456 structure. Mineralogical Magazine, 32, 261-281.

457 Young, R.A. (1993) Introduction to the Rietveld method: In: Young RA (ed) The Rietveld method.
458 Oxford, pp 1-38.

459

Figure Captions

FIGURE 1. Above: experimental (dots) and total calculated (continuous); middle: calculated erionite; bottom: difference plot of the refinement of erionite-Na from Durkee, Oregon: **a**) refinement with an isotropic crystallites shape; **b**) refinement with an anisotropic crystallites shape. Vertical bars refer to the position of the Bragg reflections. Onset: shape of the ellipsoid shape and corresponding r_a and r_c principal radii.

FIGURE 2. FESEM images of woolly erionite-Na. Bundles of fibers (**a**) and fibrils (**b,c**).

FIGURE 3. Preliminary SEM-EDX spectrum of bundles of erionite-Na. The S and Au peaks arise from, respectively, the stub adhesive and the coating.

FIGURE 4. SEM-EDX spectrum of dispersed fibers of erionite-Na.

FIGURE 5. FESEM images of small particles associated with erionite-Na fibers.

FIGURE 6. SEM-EDX spectrum of small particles occurring with erionite-Na fibers.

FIGURE 7. Ca1 site coordination (CrystalMaker 8.7; CrystalMaker Software 2012).

FIGURE 8. Ca2 site coordination (CrystalMaker 8.7; CrystalMaker Software 2012).

FIGURE 9. Ca3 site coordination (CrystalMaker 8.7; CrystalMaker Software 2012).

TABLE 1. Chemical data of erionite-Ca from Faedo, Colli Euganei, Italy as obtained from SEM-EDX and EMPA. Crystal chemical formula calculated on the basis of 36(Si+Al+Fe^{3+}) *apfu*. EMPA of Passaglia and Tagliavini (1995), labeled as P&T1995, is reported for comparison. Minimum and maximum values are reported in italics.
R = Si/(Si + Al); M = Na + K; D = Ca + Mg + Sr + Ba;
E% = 100 * $[(Al + Fe)_{ob} - Al_{th}]/Al_{th}$ where Al_{th} = Na + K + 2 * (Ca + Mg + Sr + Ba).

	P&T1995	**Present work***	
		EPMA	SEM-EDX
morphology		prismatic	
SiO_2	54.87	54.38 (*53.58-54.95*)	55.46 (*54.25-56.01*)
Al_2O_3	16.77	16.45 (*16.17-16.68*)	16.22 (*16.17-16.43*)
TiO_2	-	0.07 (*0.00-0.09*)	-
SrO	0.12	0.02 (*0.00-0.27*)	-
BaO	0.02	0.08 (*0.00-0.24*)	-
CaO	6.72	6.95 (*6.62-7.47*)	6.38 (*5.90-7.24*)
MnO	-	0.06 (*0.00-0.26*)	-
MgO	0.05	0.11 (*0.05-0.19*)	0.12 (*0.00-0.22*)
Na_2O	0.32	0.12 (*0.04-0.30*)	0.12 (*0.00-0.30*)
K_2O	2.62	3.22 (*2.89-3.51*)	3.17 (*2.60-3.90*)
H_2O	18.50	18.50	18.50
total	100	100	100
Unit-cell atomic content			
Si	26.45	26.53 (*26.43-26.58*)	26.76 (*26.71-26.77*)
Al	9.54	9.47 (*9.34-9.62*)	9.24 (*9.15-9.32*)
Ti	-	0.02 (*0.00-0.09*)	
Sr	0.01	0.01 (*0.00-0.08*)	-
Ba	-	0.02 (*0.00-0.04*)	-
Ca	3.47	3.64 (*3.45-3.96*)	3.30 (*3.05-3.83*)
Mn		0.03 (*0.00-0.11*)	-
Mg	0.04	0.08 (*0.04-0.14*)	0.09 (*0.00-0.16*)
Na	0.30	0.11 (*0.04-0.29*)	0.11 (*0.00-0.28*)
K	1.62	2.00 (*1.80-2.21*)	1.95 (*1.59-2.53*)
O	71.73	72.14	71.80 (*71.53-72.44*)
H_2O	29.81	30.17	29.84
R	0.735	0.737	0.743 (*0.741-0.746*)
M/(M+D)	0.539	0.562	0.609
Na/M	0.155	0.053	0.054
E%	5.8	-1.4	4.4

*Mean values renormalized hypothesizing a water content of 18.5 wt.%.

TABLE 2. Experimental details of XRPD data collection.

Instrument	Bruker AXS D8 Advance
Radiation	CuKα
Primary and secondary radius (mm)	250
Detector	PSD VÅNTEC-1
Sample mount	Rotating capillary (60 r/min)
Incident beam optics	60 mm multilayer (Göbel) X-ray mirror
Detector window (°)	6
Divergence slits (°)	0.3
Soller slits	Primary beam (2.3°); diffracted beam (radial)
Angular range (°2θ)	4-145
$(\sin \theta/\lambda)_{max}$ ($Å^{-1}$)	0.619
Step size (°2θ)	0.022
Counting time (s)	10

TABLE 3. Results of quantitative SEM-EDX microanalyses of erionite from Durkee, Oregon. Chemical analyses of reference samples are reported for comparison.

	1	2	3	**present work***
morphology	woolly	woolly	acicular/ prismatic	woolly
SiO_2	57.16	57.40	58.35	58.74 (*58.17-59.36*)
Al_2O_3	16.08	15.60	13.32	13.46 (*13.19-13.83*)
Fe_2O_3	-	-	0.16	-
BaO	-	-	0.68	-
CaO	3.50	2.92	4.11	-
MgO	0.66	1.11	0.83	0.33 (*0.14-0.54*)
Na_2O	2.47	1.45	0.36	5.75 (*4.78-6.44*)
K_2O	3.51	3.40	2.72	3.22 (*2.69-3.67*)
TiO_2	-	-	-	-
P_2O_5	-	-	-	-
MnO	-	-	-	-
H_2O	17.30	17.58	19.47	18.50
total	100.68	99.46	100.30	100.00
Unit-cell atomic content				
Si	27.04	27.27	28.31	28.34 (*28.24-28.44*)
Al	8.96	8.73	7.61	7.66 (*7.56-7.76*)
Fe^{3+}	-	-	0.06	-
Fe^{2+}	-	-	-	
Ba	-	-	0.13	-
Ca	1.77	1.49	2.14	-
Mg	0.47	0.79	0.60	0.24 (*0.10-0.38*)
Na	2.27	1.34	0.34	5.38 (*4.43-6.05*)
K	2.12	2.06	1.68	1.98 (*1.66-2.29*)
O	71.95	71.60	72.16	72.09 (*71.69-72.39*)
H_2O	27.29	27.85	31.57	29.77
R	0.751	0.757	0.787	0.787 (*0.784-0.790*)
M/(M+D)	0.662	0.599	0.425	0.969
Na/M	0.517	0.333	0.168	0.731
E%	1.2	10.0	-0.9	-2.3
species	-Na	-K	-Ca	-Na

*Mean values, from 16 analytical points renormalized hypothesizing a water content of 18.5 wt.%.

1. Chemical analysis by Eakle (1898).
2. Chemical analysis by Staples and Gard (1959).
3. Chemical analysis of sample no. 25, by Passaglia et al. (1998).

TABLE 4. Comparison of cell parameters of erionite samples from Durkee.

	1	2	**present work**
morphology	woolly	acicular/ prismatic	woolly
a (Å)	13.254(6)	13.233(1)	13.2357(5)
c (Å)	15.100(10)	15.055(4)	15.0652(6)
Vol. (Å^3)	2297(3)	2283.1(6)	2285.6(2)
c/a	1.1393(12)	1.1377(4)	1.1382(1)
species	-Na	-Ca	-Na

1. Sheppard and Gude (1969) recalculated from the original *d*-spacings of Staples and Gard (1959).
2. Passaglia et al. (1998): sample no. 25.

TABLE 5. Fractional coordinates, isotropic displacement parameters, site multiplicity and occupancy, and site scattering (*s.s.*) of erionite-Na. Si, Al site partition from Jones' (1968) determinative curves.

Site	*Site mult.*	*x*	y	z	B_{iso}(Å^2)	Site occ.	s.s.(e$^-$)	Proposed site partition	s.s.(e$^-$) from site partition
				Framework					
T1	24	0.2331(3)	0.0001(4)	0.10454(16)	0.88(5)	1		$Si_{19.79}Al_{4.21}$	
T2	12	0.0958(4)	0.4246(5)	1/4	0.88(5)	1		$Si_{8.74}Al_{3.26}$	
O1	24	0.3483(5)	0.0239(5)	0.6604(5)	1.34(13)	1			
O2	12	0.1005(4)	2*x*	0.1269(7)	1.34(13)	1			
O3	12	0.1270(3)	2*x*	0.6402(8)	1.39(19)	1			
O4	12	0.2634(6)	0	0	1.34(13)	1			
O5	6	0.2307(6)	2*x*	1/4	1.39(19)	1			
O6	6	0.4616(7)	2*x*	1/4	1.39(19)	1			
				EF cations					
Ca1	4	1/3	2/3	0.924(16)	12.3(13)	0.112(29)	5.4(14)	$Mg_{0.24}$	2.9
Ca2	4	1/3	2/3	0.0893(15)	12.3(13)	0.806(23)	35.5(10)	$Na_{3.48}$	38.3
Ca3	4	1/3	2/3	0.7068(28)	12.3(13)	0.44(3)	19.4(14)	$Na_{1.90}$	20.9
K1	2	0	0	1/4	2.63(24)	1	38	$K_{1.99}$	37.8
						$\Sigma_{cat.}$	98(4)		99.9
				Water molecules					
OW7	6	0.2375(14)	2*x*	3/4	5.0(3)	0.641(22)	30.8(11)		
OW8	12	0.2565(18)	2*x*	0.9674(28)	9.9(6)	0.404(17)	38.8(16)		
OW9	12	0.498(5)	2*x*	0.950(4)	9.9(6)	0.239(18)	22.9(17)		
OW10	12	0.4365(13)	2*x*	0.6601(16)	9.9(6)	0.565(15)	54.2(14)		
OW11	12	0.2707(26)	2*x*	0.647(4)	9.9(6)	0.363(24)	34.8(23)		
OW12	12	0.4365(13)	2*x*	0.050(17)	9.9(6)	0.704(23)	67.6(22)		
						Σ_{water}	249(10)		

TABLE 6. Relevant bond distances (Å) and angles (°) of erionite-Na from Durkee, Oregon. In italic never occurring short distances.

T1-O2	1.622(5)	O1-T1-O2	109.7(5)
T1-O4	1.625(3)	O1-T1-O3	105.5(4)
T1-O1	1.629(9)	O1-T1-O4	107.0(5)
T1-O3	1.649(7)	O2-T1-O3	109.2(5)
<T1-O>	1.631	O2-T1-O4	111.5(4)
		O3-T1-O4	113.6(5)
T2-O5	1.598(7)	O1-T2-O1	107.9(5)
T2-O6	1.647(8)	O1-T2-O5 x2	113.4(5)
T2-O1 x2	1.670(7)	O1-T2-O6 x2	104.6(5)
<T2-O>	1.646	O5-T2-O6	112.3(7)
T1-O1-T2	140.3(6)	T1-O4-T1	151.4(6)
T2-O2-T1	144.2(7)	T2-O5-T2	149.4(11)
T1-O3-T1	138.2(8)	T2-O6-T2	164.8(11)
K1-O2 x6	2.957(10)		
K1-O3 x6	3.348(9)		
Ca1-OW11x3	*1.79(16)*	Ca1-Ca3	*1.97(24)*
Ca1-OW8 x3	1.88(9)	Ca1-Ca2	*2.49(24)*
Ca1-OW12 x3	2.66(12)	OW8-OW11	*1.75(7)*
Ca1-OW10 x3	*2.68(12)*		
Ca2-OW8 x3	2.54(4)		
Ca2-OW12	2.68(3)		
Ca2-O5 x3	3.376(19)		
Ca3-OW11x3	*1.70(6)*	Ca3-Ca3	*1.30(8)*
Ca3-OW7 x3	*2.29(3)*	OW7-OW11	*1.73(6)*
Ca3-OW10 x3	2.47(3)		
Ca3-OW11 x3	2.64(7)		
Ca3-OW10 x3	3.10(4)		
Ca3-OW8 x3	3.16(5)		
		OW9-OW9	*1.51(13)*
		OW9-OW12	*1.63(10)*
		OW9-OW12	*1.66(10)*

TABLE 7. Bond valence analysis (*v.u.*) following Breese and O'Keeffe (1991).

	K	Na	Mg
K1-O2 x6	0.107 x6		
K1-O3 x6	0.037 x6		
Σ	0.864		
Ca1-OW8 x3			0.607 x3
Ca1-OW10 x3			0.069 x3
Σ			2.028
Ca2-OW8 x3		0.134 x3	
Ca2-OW12 x3		0.092 x3	
Ca2-O5 x3		0.014 x3	
Σ		0.720	
Ca3-OW10 x3		0.164 x3	
Ca3-OW11 x3		0.105 x3	
Ca3-OW10 x3		0.030 x3	
Σ		0.897	

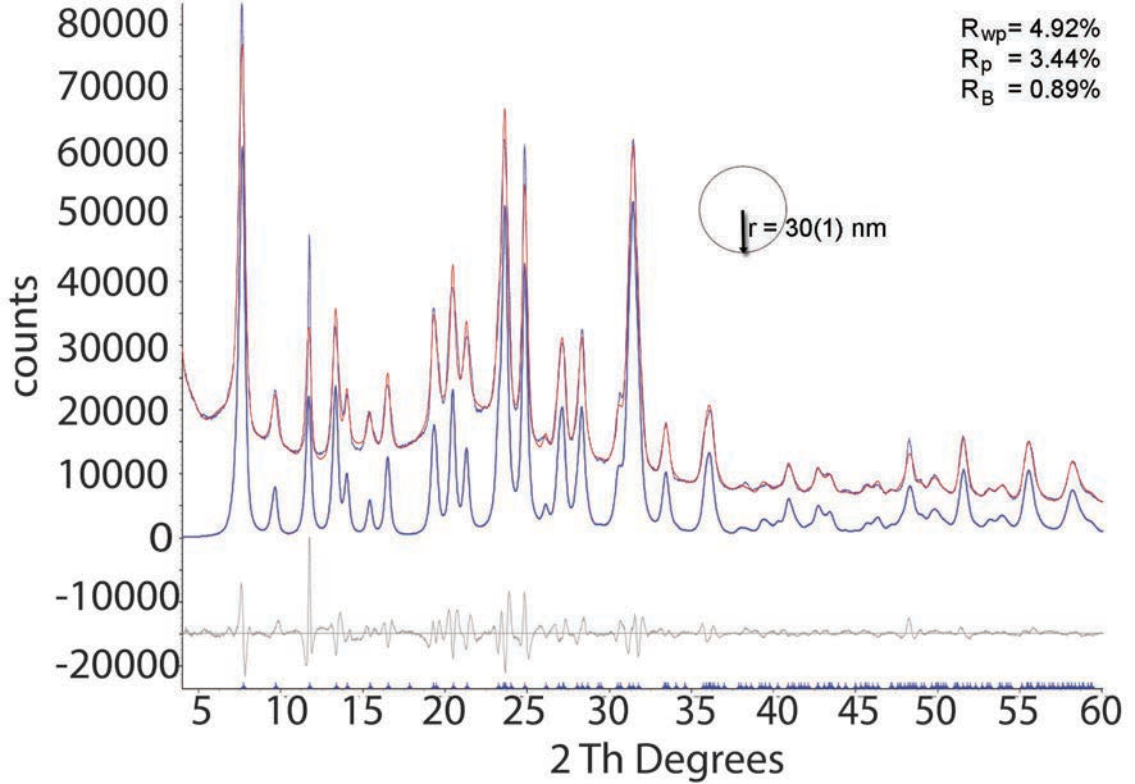
80000
70000
60000
50000
40000
30000
20000
10000
0
-10000
-20000
counts
5
10
15
20
25
30
35
40
45
50
55
60
2 Th Degrees
R_{wp}= 4.92%
R_p = 3.44%
R_B = 0.89%
r = 30(1) nm

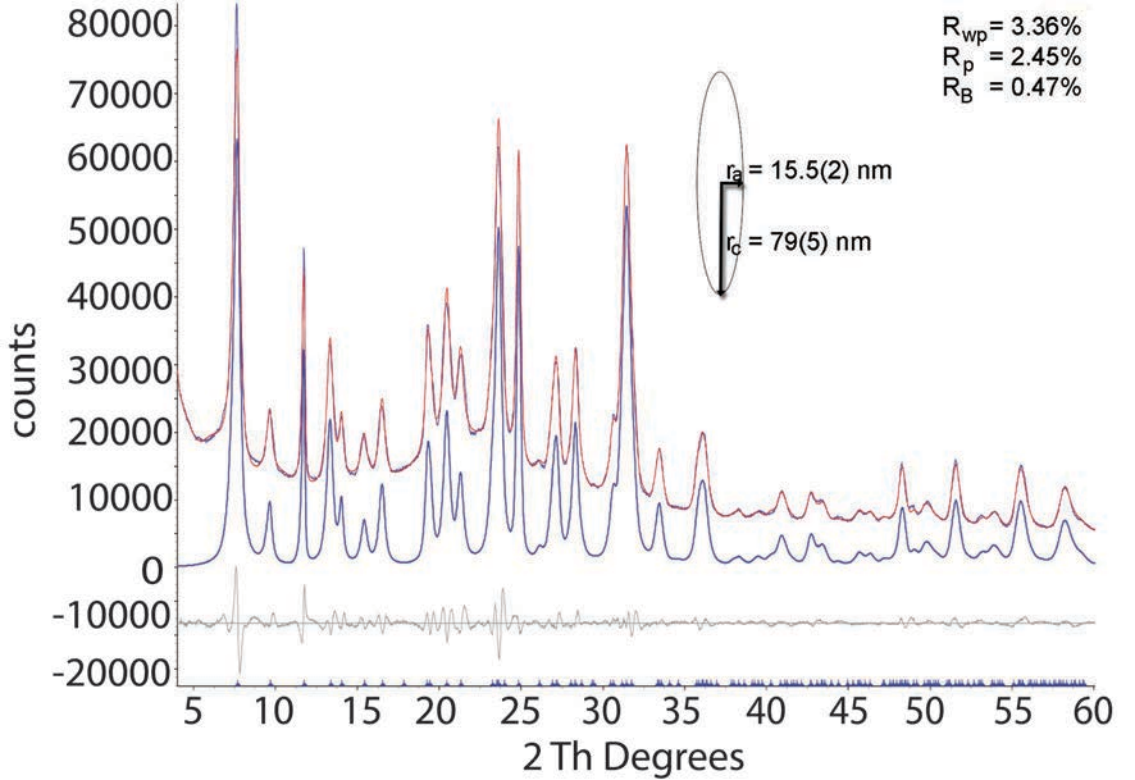
80000
70000
60000
50000
40000
30000
20000
10000
0
-10000
-20000
counts
5
10
15
20
25
30
35
40
45
50
55
60
2 Th Degrees
R_{wp} = 3.36%
R_p = 2.45%
R_B = 0.47%
r_a = 15.5(2) nm
r_c = 79(5) nm

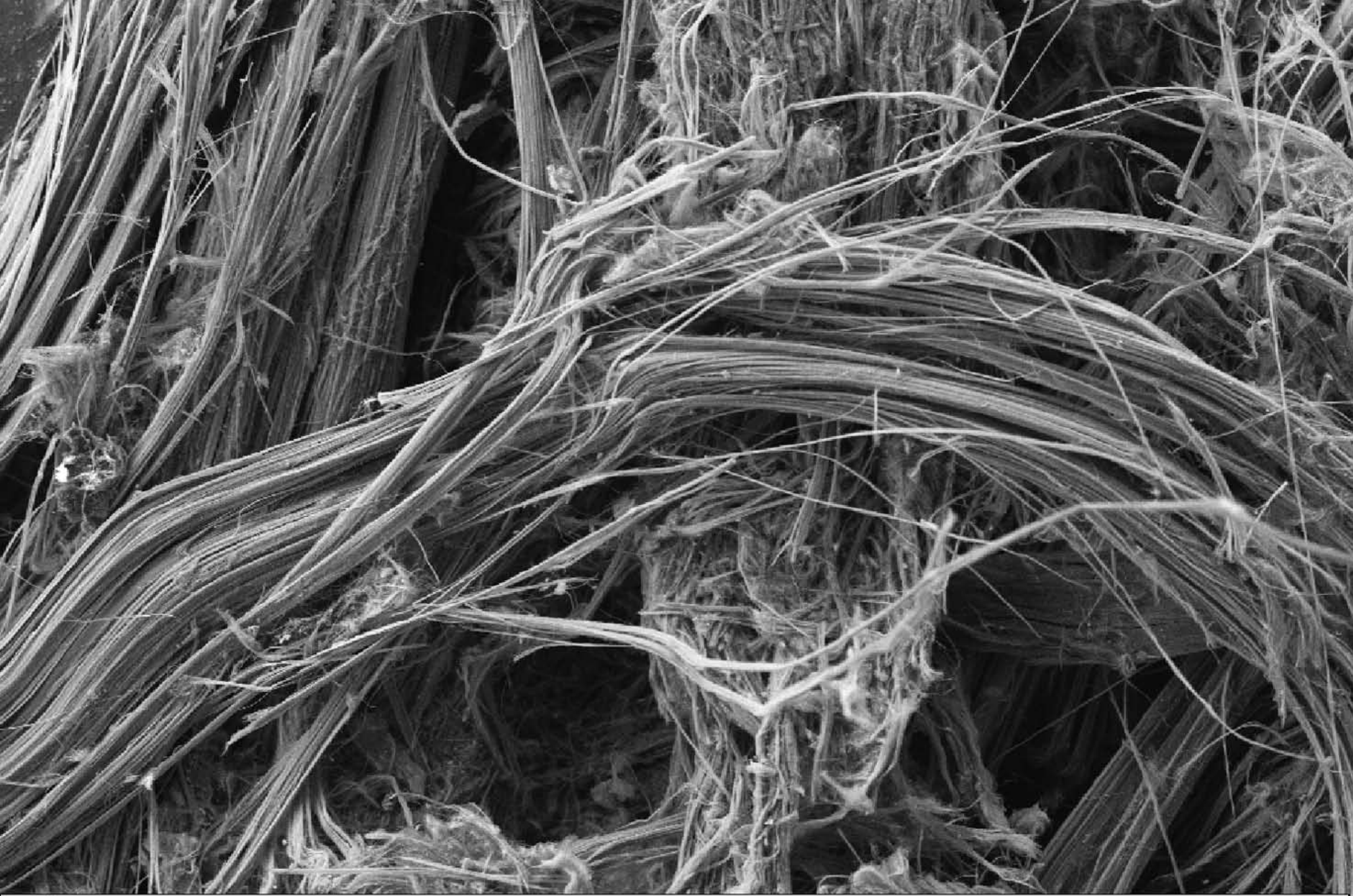
10 µm
EHT = 6.00 kV
WD = 3.5 mm
Signal A = SE2
Mag = 1.00 K X
Date :24 Feb 2012
Sample ID = Ballirano
CNIS

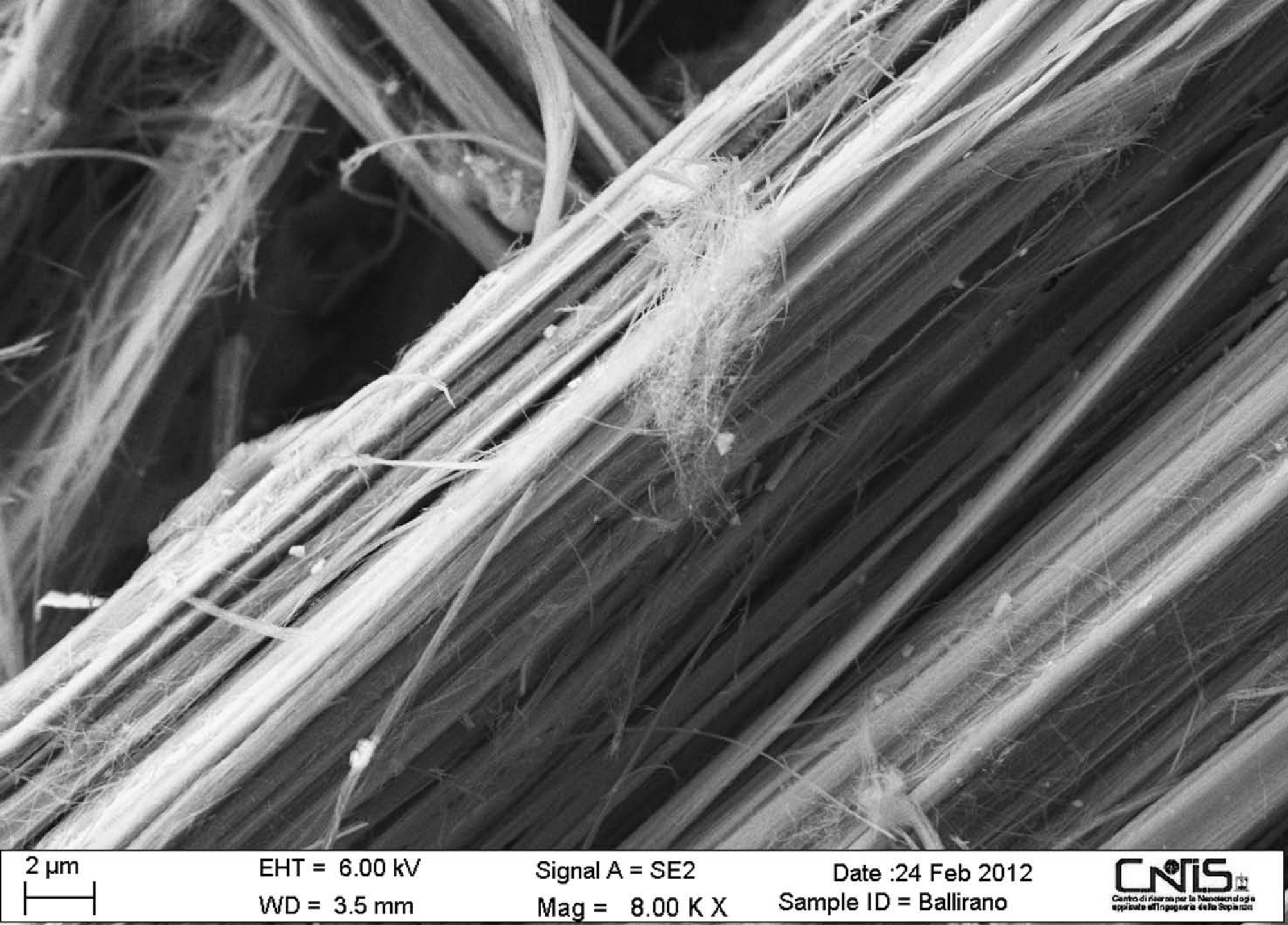
2 µm
EHT = 6.00 kV
WD = 3.5 mm
Signal A = SE2
Mag = 8.00 K X
Date :24 Feb 2012
Sample ID = Ballirano
CNIS
Centro di ricerca per le Nanotecnologie applicate all'Ingegneria della Sapienza

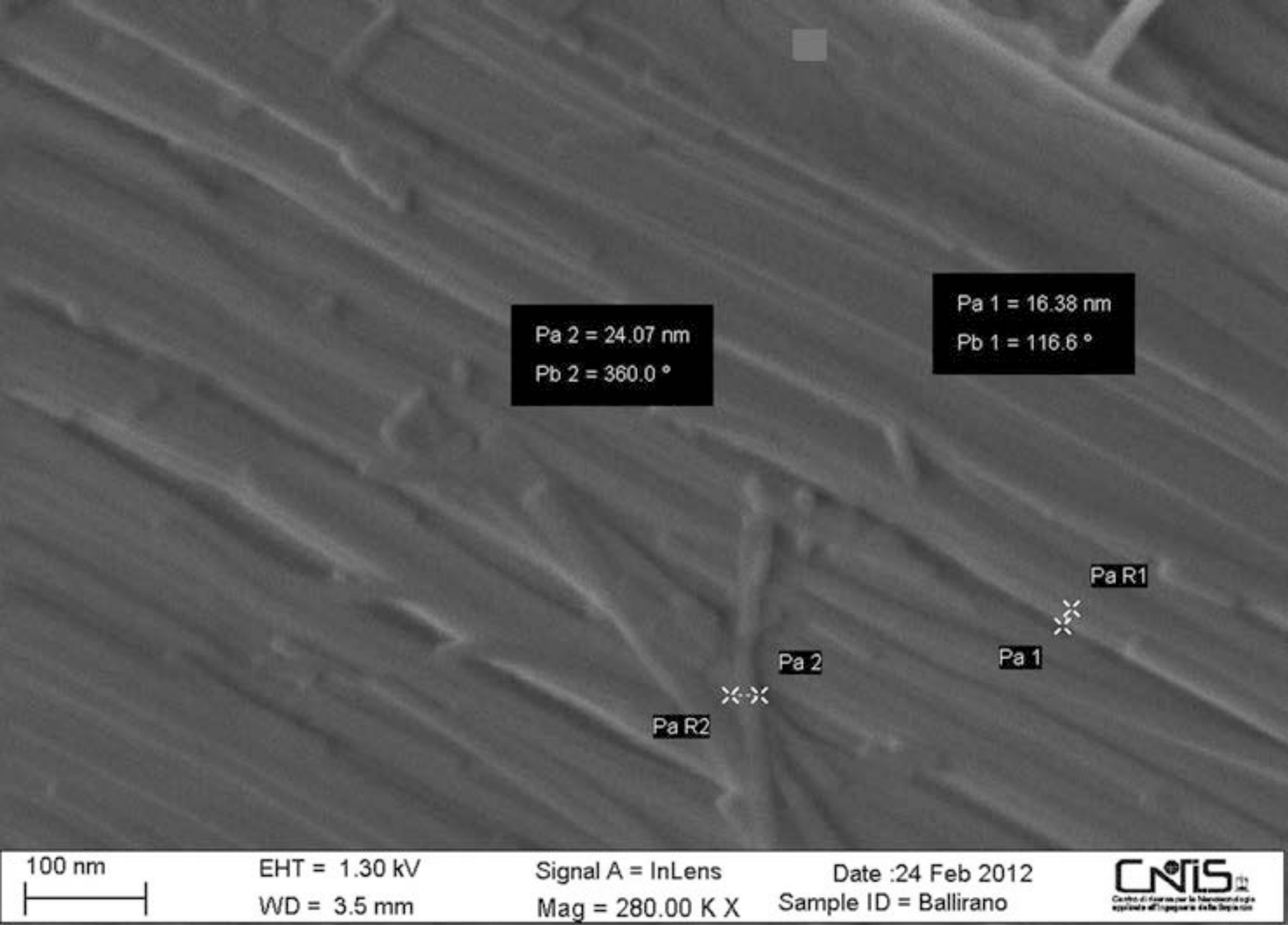
Pa 2 = 24.07 nm
Pb 2 = 360.0 °
Pa 1 = 16.38 nm
Pb 1 = 116.6 °
Pa R1
Pa 1
Pa 2
Pa R2
100 nm
EHT = 1.30 kV
WD = 3.5 mm
Signal A = InLens
Mag = 280.00 K X
Date :24 Feb 2012
Sample ID = Ballirano

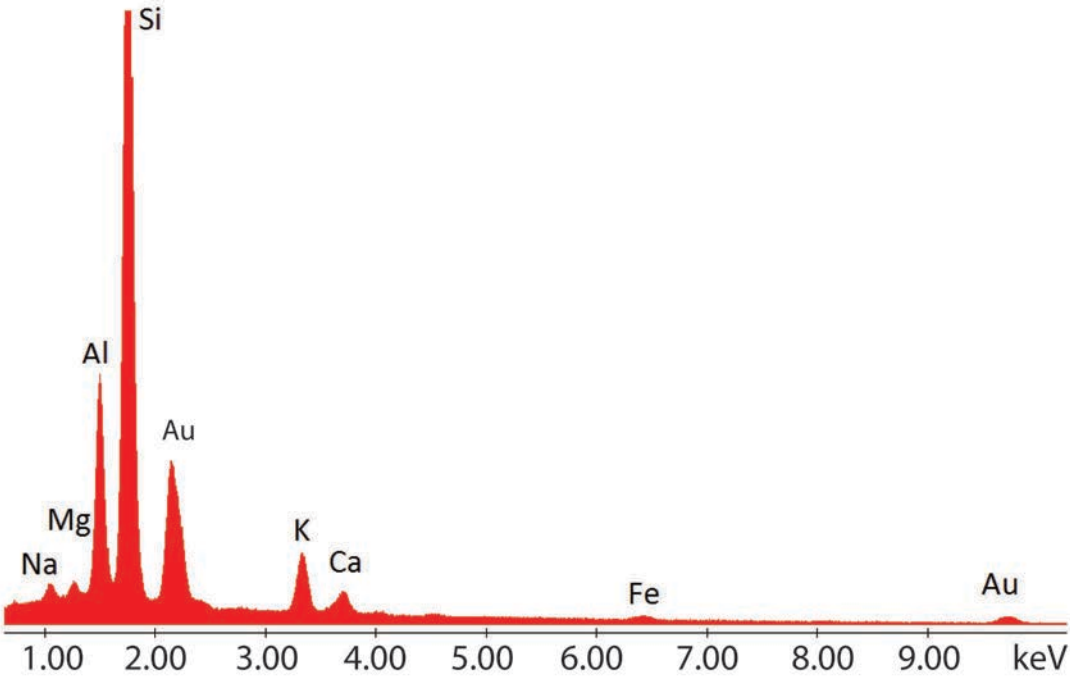
Si
Al
Au
Mg
K
Na
Ca
Fe
Au
1.00
2.00
3.00
4.00
5.00
6.00
7.00
8.00
9.00
keV

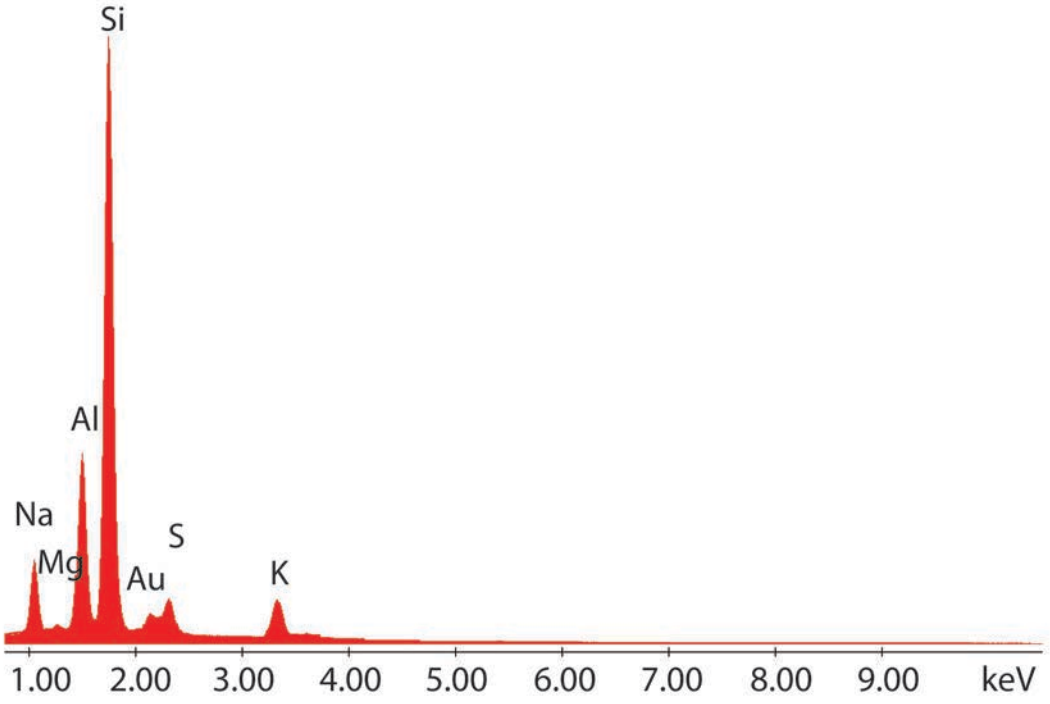
Si
Al
Na
Mg
Au
S
K
1.00
2.00
3.00
4.00
5.00
6.00
7.00
8.00
9.00
keV

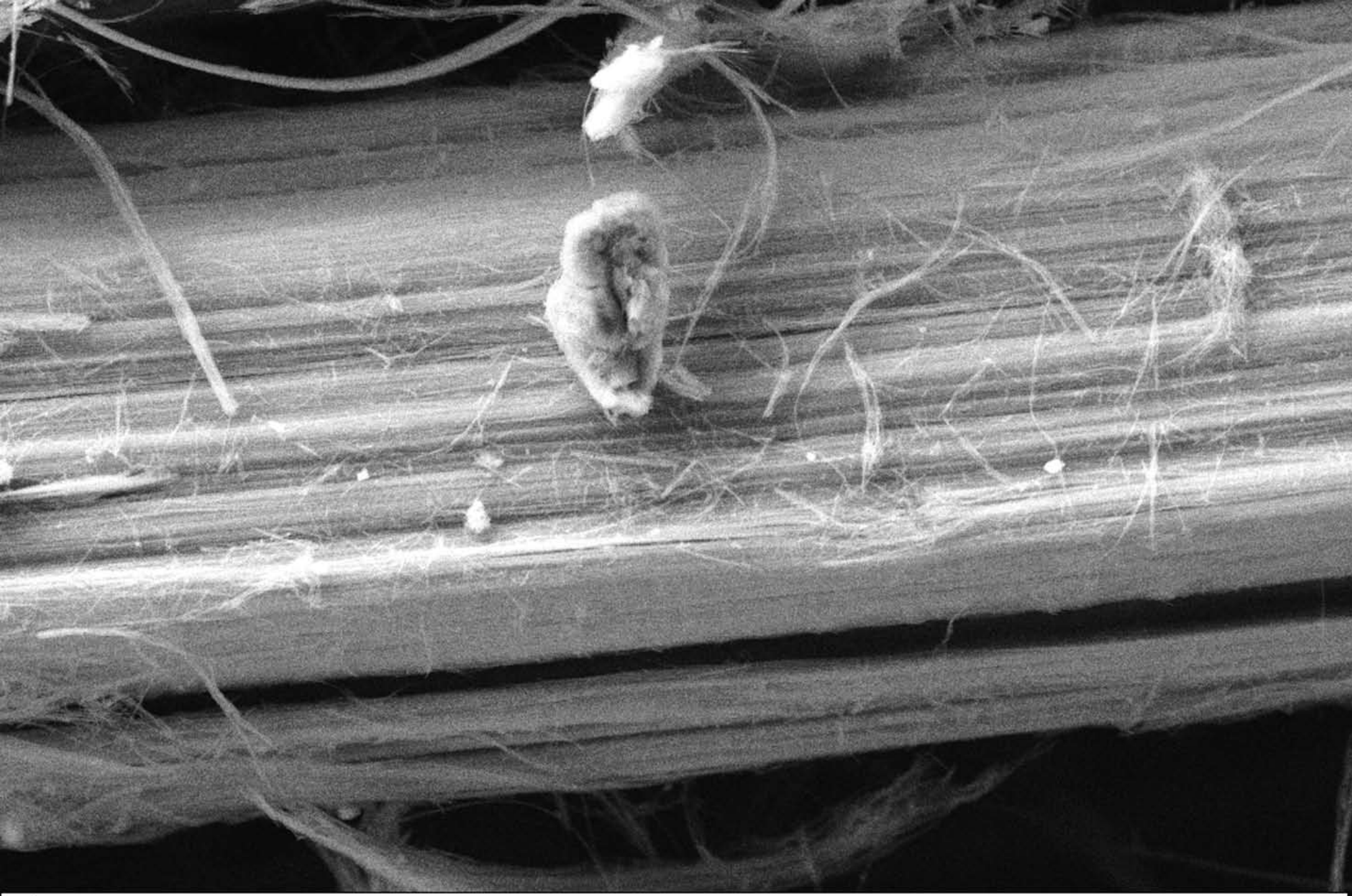
1 µm
EHT = 5.00 kV
WD = 2.8 mm
Signal A = SE2
Mag = 15.00 K X
Date :24 Feb 2012
Sample ID = Ballirano
CNIS
Centro di ricerca per la Nanotecnologia applicata all'Ingegneria della Sapienza

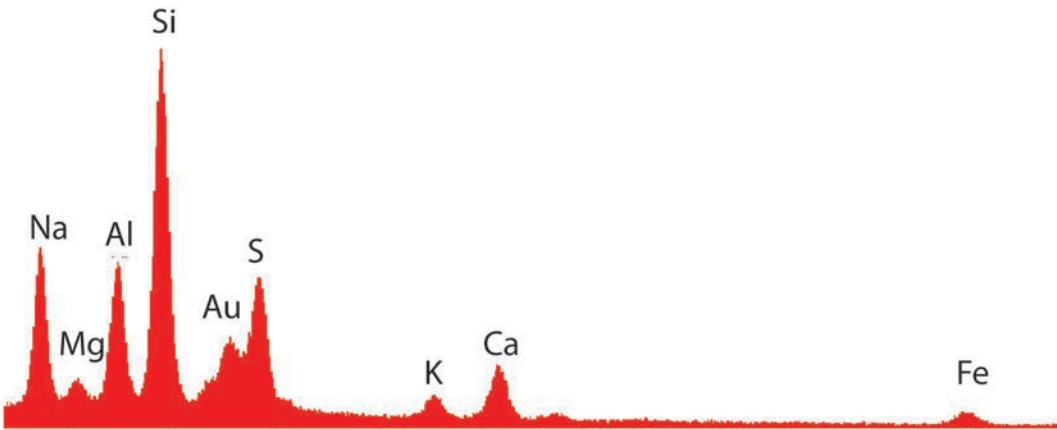
Si
Na
Al
S
Au
Mg
K
Ca
Fe
1.20
1.80
2.40
3.00
3.60
4.20
4.80
5.40
6.00
keV

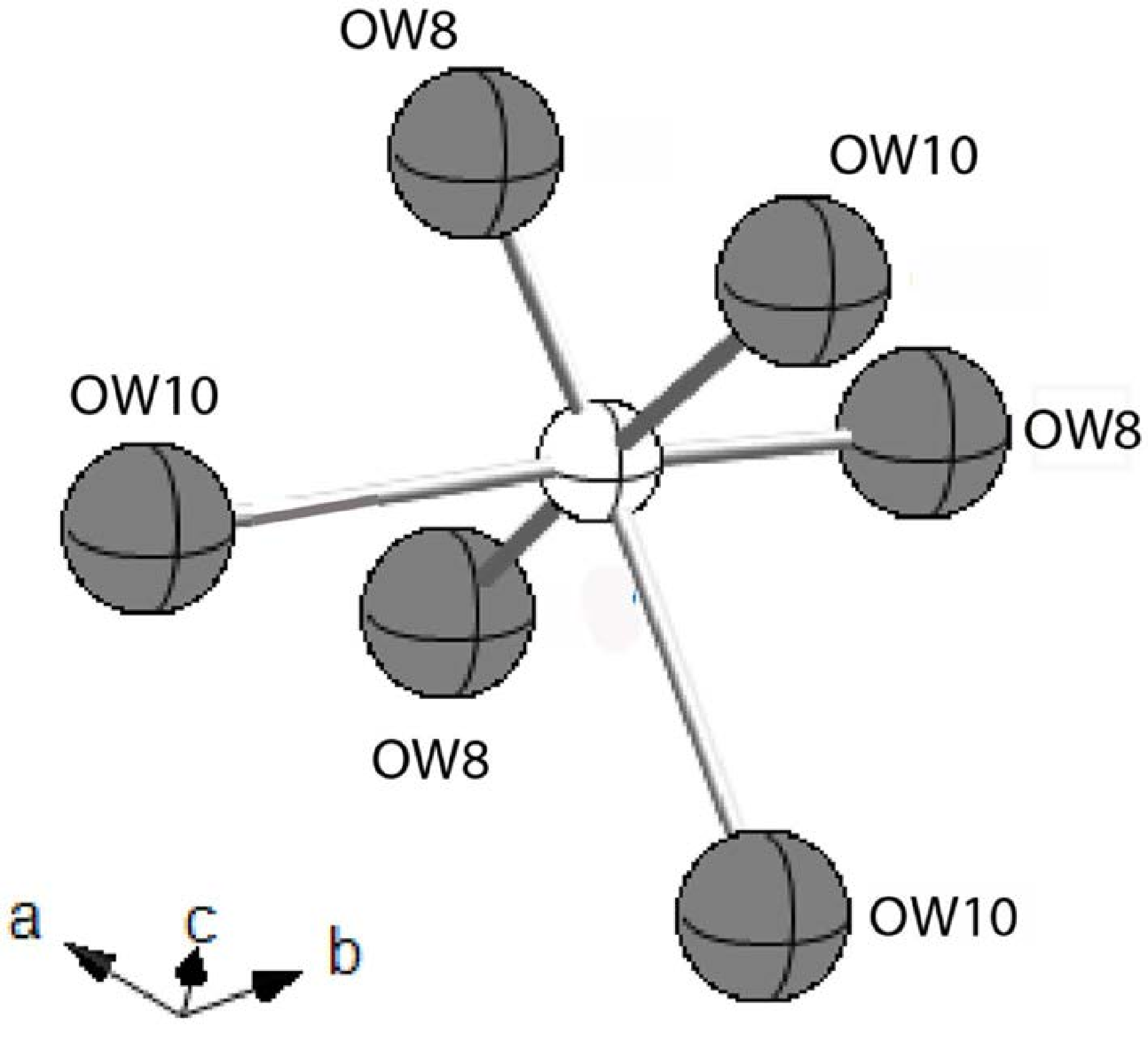
OW8
OW10
OW10
OW8
OW8
OW10
a
c
b

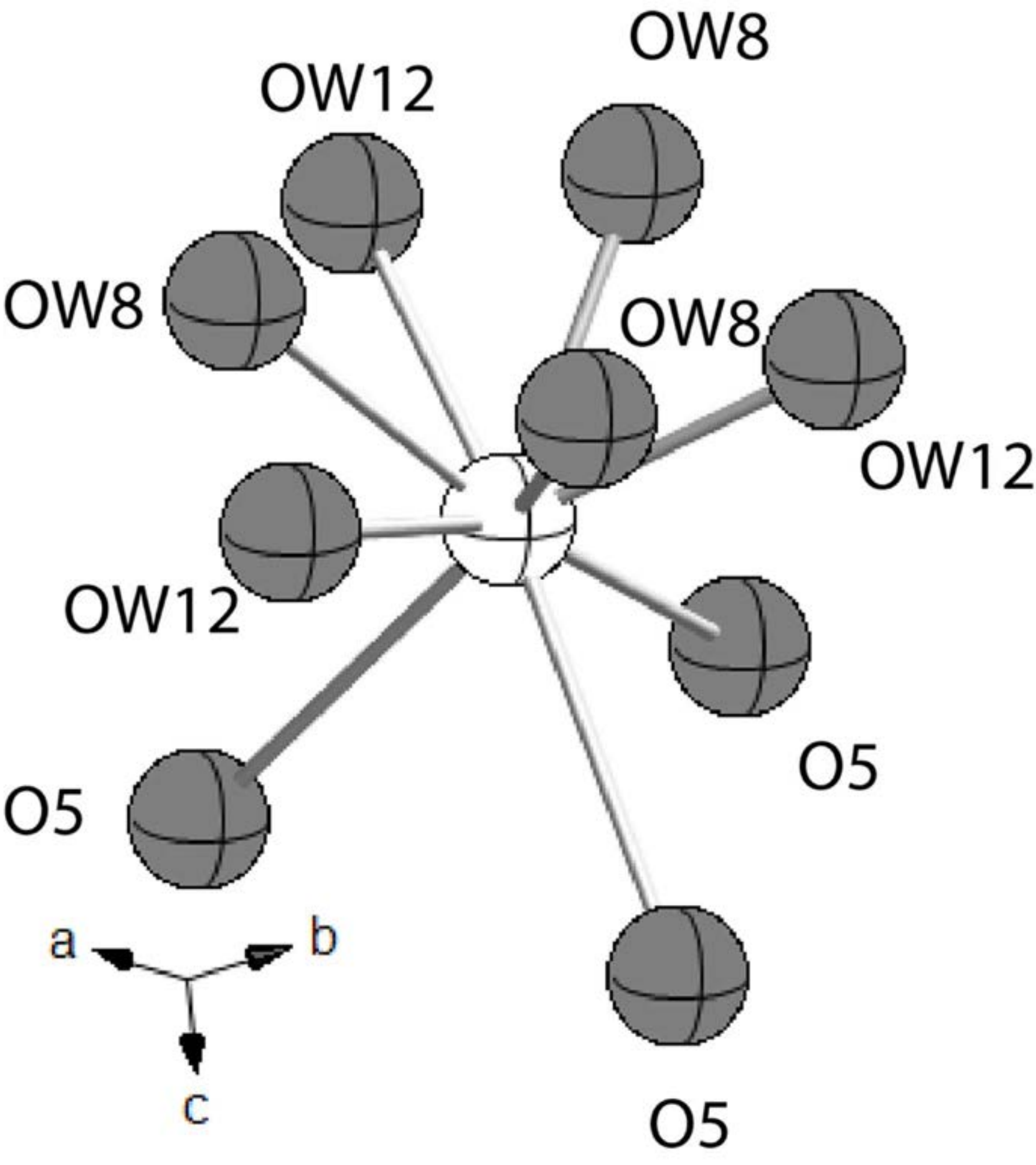
OW8
OW12
OW8
OW8
OW12
OW12
O5
O5
O5
a
b
c

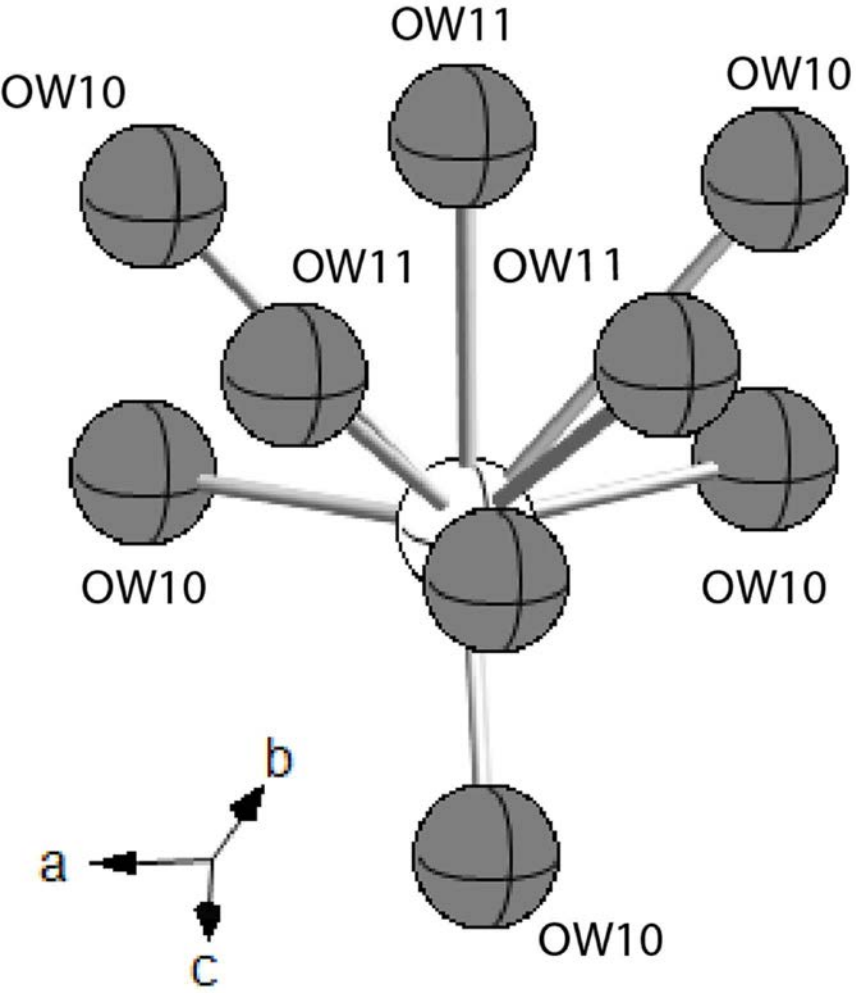
OW11
OW10
OW10
OW11
OW11
OW10
OW10
OW10
b
a
c